Article

Discovery Medicine 2026; 38(212): 2931–2946
https://doi.org/10.24976/Discov.Med.202638212.226

NCKAP1 Is Essential for SLC7A11-Dependent Disulfide Stress-Induced Cell Death Under Glucose Starvation in an Oral Squamous Cell Model

Weiwei He[1,*], Sai Ma[1], Weilong Lin[1], Jiarui Hu[2], Yingpeng Su[3], Jiashuo Yang[1]

[1]Department of Stomatology, The First Affiliated Hospital of Hebei North University, 075000 Zhangjiakou, Hebei, China
[2]Department of Traditional Chinese Medicine, The First Affiliated Hospital of Hebei North University, 075000 Zhangjiakou, Hebei, China
[3]Central Laboratory, The First Affiliated Hospital of Hebei North University, 075000 Zhangjiakou, Hebei, China
*Correspondence: gege13993@126.com (Weiwei He)
Submitted: 13 July 2026 Revised: 14 August 2026 Accepted: 25 August 2026 Published: 23 September 2026

Background: Oral squamous cell carcinoma (OSCC) has a poor prognosis and requires new therapeutic strategies. Disulfidptosis is a recently defined form of cell death that occurs in SLC7A11-high cells under glucose starvation and has been linked to collapse of the actin cytoskeleton. NCKAP1 has been linked to this process in other tumors, but its role in OSCC remains unknown. The aim of this study was to determine whether NCKAP1 mediates glucose-starvation-induced, disulfide stress-driven cell death in an OSCC cell model and to examine whether its contribution depends on SLC7A11-mediated cystine import.

Methods: Expression of NCKAP1 and SLC7A11 was assessed in OSCC cell lines and normal oral keratinocytes by qRT-PCR and Western blotting. A glucose-starvation model was established in SCC-9 cells, and the resulting cell death was characterized using cell viability assays, lactate dehydrogenase (LDH) release assays, flow cytometry, a panel of death-pathway inhibitors, and reducing agents. NCKAP1 was manipulated using siRNA, plasmid overexpression, and stable shRNA knockdown. Features of disulfide stress were evaluated by measuring free thiols and NADPH/$NADP^+$ levels, as well as by analyzing the glutathione pool, including total glutathione, oxidized glutathione (GSSG), reduced glutathione (GSH) and the GSH/GSSG ratio. Proliferation and migration were assessed using colony formation, wound healing, and transwell assays.

Results: NCKAP1 and SLC7A11 were higher in the two OSCC cell lines examined than in normal keratinocytes, each cultured in its respective routine medium ($p < 0.001$). In SCC-9 cells, glucose starvation triggered a rapid, non-apoptotic death that was not inhibited by inhibitors of apoptosis, necroptosis, autophagy, or ferroptosis, but was largely prevented by co-treatment with dithiothreitol (DTT) and tris(2-carboxyethyl)phosphine (TCEP) ($p < 0.001$). This response was accompanied by decreased NADPH/$NADP^+$ ratios, depletion of the glutathione pool with GSSG accumulation, an approximately 89% reduction in the GSH/GSSG ratio, and loss of free thiols (all $p < 0.001$). NCKAP1 knockdown preserved cell viability and partially preserved intracellular free thiols, whereas NCKAP1 overexpression aggravated thiol depletion ($p < 0.001$). NCKAP1 overexpression failed to reduce cell viability when SLC7A11 was silenced. Manipulation of NCKAP1 did not materially alter total glutathione or GSSG, but produced modest changes in reduced GSH, the GSH/GSSG ratio and, after knockdown, the NADPH/$NADP^+$ ratio, recovering less than 10% of the starvation-induced changes. These data argue against a major role of NCKAP1 in the upstream redox collapse without excluding a minor metabolic contribution, and are consistent with a functional dependency in which the contribution of NCKAP1 requires SLC7A11-mediated cystine import. Under normal culture conditions, NCKAP1 knockdown also reduced colony formation, wound closure, and migration (all $p < 0.001$).

Conclusion: NCKAP1 is required for glucose-starvation-induced, disulfide stress-driven cell death and contributes to SCC-9 proliferation and migration, identifying the Wiskott-Aldrich syndrome protein (WASP)-family verprolin-homologous protein (WAVE) regulatory complex component NCKAP1 as a factor involved in this death modality.

Keywords: OSCC; disulfide stress; NCKAP1; SLC7A11; WAVE regulatory complex; glucose starvation

Introduction

Oral squamous cell carcinoma (OSCC) is the most common malignancy of the oral cavity, accounting for approximately 90% of oral cancers [1,2]. Despite advances in treatment, including surgery, radiotherapy, and chemotherapy, the prognosis of patients with advanced disease remains poor [3,4]. Local recurrence and metastasis remain frequent. In population-based cohorts restricted to the oral cavity, five-year survival rates remain close to 50%. Overall and disease-specific survival rates were 47% and 52%, respectively, in a Norwegian national cohort, while five-year relative survival was 54.6% in a German registry study, declining to approximately one third in patients with stage IV disease [5,6]. These findings underscore the need for

Copyright: © 2026 The Author(s). Published by Discovery Medicine. This is an open access article under the CC BY 4.0 license.
Note: *Discovery Medicine* stays neutral with regard to jurisdictional claims in published maps and institutional affiliations.

therapeutic strategies beyond current treatment approaches [7]. One promising direction is to exploit the metabolic vulnerabilities of tumor cells [8,9,10].

Regulated cell death has emerged as an important target in cancer therapy [11,12]. Beyond apoptosis, several non-apoptotic cell death modalities have been described, including necroptosis, ferroptosis, and autophagy-dependent cell death [13,14,15]. Disulfidptosis is a more recently defined form of regulated cell death [16,17]. It occurs in cells with high expression of the cystine transporter SLC7A11 under glucose-deprived conditions [16,17]. Many tumor types upregulate SLC7A11, making disulfidptosis a potentially relevant therapeutic vulnerability in cancer [17,18].

SLC7A11 imports cystine, which must be reduced to cysteine using NADPH [19]. A major source of cellular NADPH is the glucose-dependent pentose phosphate pathway (PPP) [20]. When glucose is withdrawn, NADPH becomes insufficient, leading to cystine accumulation and aberrant disulfide-bond formation [21]. These bonds form within actin cytoskeletal proteins, disrupting the F-actin network, cell contraction, and cell detachment, ultimately resulting in cell death [21]. This places the actin cytoskeleton at the core of this death process.

The organization of the actin cytoskeleton is controlled by dedicated regulatory complexes. The Wiskott-Aldrich syndrome protein (WASP)-family verprolin-homologous protein (WAVE) regulatory complex (WRC) couples Ras-related C3 botulinum toxin substrate 1 (Rac1) signaling to Arp2/3-mediated actin branching [22,23]. NCKAP1 is a core component of this complex [24]. Through the WAVE-Arp2/3 axis, NCKAP1 contributes to lamellipodia formation and cell motility [24,25]. Altered NCKAP1 expression has been reported in several cancers [26]. Consistent with its cytoskeletal role, the genome-wide screen that originally defined disulfidptosis identified the Rac-WRC axis as a key regulator of disulfide stress-induced cell death; loss of WRC activity, including NCKAP1 depletion, partially protected renal cancer cells from disulfide stress [16]. Whether this dependency operates in oral squamous cell carcinoma, how NCKAP1 functionally relates to SLC7A11 within this pathway, and whether NCKAP1 contributes to OSCC proliferation and migration beyond the context of cell death remain unaddressed.

In this study, we examined the expression of NCKAP1 and SLC7A11, established a glucose-starvation model, characterized the resulting cell death, and tested whether NCKAP1 influences this process and where it acts within the pathway. We also assessed the effects of NCKAP1 on OSCC proliferation and migration under normal culture conditions. Our aim was to clarify the role of NCKAP1 in OSCC disulfide stress-driven cell death and malignant behavior.

Materials and Methods

Cell Lines and Culture Conditions

SCC-9 (CRL-1629) and CAL-27 (CRL-2095) human OSCC cells were obtained from the American Type Culture Collection (ATCC, Manassas, VA, USA), and normal human oral keratinocytes (HOK, 2610) were purchased from ScienCell Research Laboratories (Carlsbad, CA, USA). SCC-9 cells were propagated in DMEM/F12 (1:1; Gibco, Thermo Fisher Scientific, Grand Island, NY, USA, #11320033) containing 10% fetal bovine serum (FBS; Gibco, #10099141), 1% penicillin/streptomycin (P/S; Gibco, #15140122) and 400 ng/mL hydrocortisone (Sigma-Aldrich, St. Louis, MO, USA, #H0888). CAL-27 cells were grown in high-glucose DMEM (Gibco, #11965092) supplemented with 10% FBS and 1% P/S. HOK cells were cultured in Oral Keratinocyte Medium (ScienCell Research Laboratories, Carlsbad, CA, USA, #2611) with the supplier-provided growth supplement. Cultures were maintained at 37 °C in 5% CO_2 under humidified conditions. All cell lines were authenticated by Short Tandem Repeat profiling and confirmed to be mycoplasma free.

To impose glucose-starvation (GF), cultures were rinsed twice with prewarmed PBS and transferred to glucose-free DMEM (Gibco, Thermo Fisher Scientific, Grand Island, NY, USA, #11966025) containing 10% dialyzed FBS (Gibco, #A3382001) and 1% P/S. Dialyzed FBS was used to minimize residual glucose. The glucose-replete control (Ctrl, designated 0 h in the time-course experiments) was the conventional complete medium in which SCC-9 cells were routinely maintained, namely DMEM/F12 (1:1) containing 10% non-dialyzed FBS, 1% P/S and 400 ng/mL hydrocortisone. A glucose add-back control prepared in the glucose-free basal medium was not used. The Ctrl and GF conditions therefore differ not only in D-glucose but also in basal formulation and in the use of dialyzed rather than non-dialyzed serum. The condition is accordingly described throughout as glucose-free culture rather than as glucose withdrawal in isolation, and this is addressed in the limitations section. For cystine-withdrawal experiments, the basal medium was DMEM (Gibco, #21013024) supplemented with 4 mM L-glutamine (Sigma-Aldrich, St. Louis, MO, USA, #G7513) and 200 µM L-methionine (Sigma-Aldrich, #M9625). The matched cystine-replete medium additionally contained 200 µM L-cystine (Sigma-Aldrich, #C7602).

Inhibitor and Reducing-Agent Treatments

Z-VAD-FMK (20 µM; MedChemExpress, Monmouth Junction, NJ, USA, #HY-16658B), Necrostatin-1 (20 µM; MedChemExpress, #HY-15760), 3-MA (5 mM; MedChemExpress, #HY-19312), Ferrostatin-1 (2 µM; MedChemExpress, #HY-100579), DTT (1 mM; Beyotime, Shanghai, China, #ST041) and TCEP (500 µM; Thermo

Fisher Scientific, Waltham, MA, USA, #77720) were added to the glucose-free medium at the onset of glucose starvation (t = 0) and were present throughout the treatment period. Thus, reducing agents were present prior to the accumulation of intracellular disulfide stress.

siRNA and Plasmid Transfection

GenePharma (Shanghai, China) synthesized siRNAs against NCKAP1 (si-NCKAP1, sense 5'-AACAUCUACAAAUGUGAAGUA-3', antisense 5'-CUUCACAUUUGUAGAUGUUAU-3') and SLC7A11 (si-SLC7A11, sense 5'-ACAAAGUUGAGGUAAAACCAG-3', antisense 5'-GGUUUUACCUCAACUUUGUUA-3'), as well as a non-targeting control (si-NC, sense 5'-UUCUCCGAACGUGUCACGUTT-3', antisense 5'-ACGUGACACGUUCGGAGAATT-3'). Cells were plated in 6-well dishes one day before transfection and exposed to 50 nM siRNA using Lipofectamine RNAiMAX (Invitrogen, Thermo Fisher Scientific, Carlsbad, CA, USA, #13778075). For NCKAP1 overexpression, the full-length human NCKAP1 coding sequence (NM_013436), verified by Sanger sequencing, was inserted into pcDNA3.1-3×Flag. Lipofectamine 3000 (Invitrogen, #L3000015) was used to deliver 2 µg Flag-NCKAP1 plasmid or the corresponding empty vector (OE-NC). Unless stated otherwise, assays were initiated 48 h after transfection.

Lentivirus Production and Generation of Stable Cell Lines

Stable NCKAP1 knockdown was generated using pLKO.1-puro vector (Addgene, Watertown, MA, USA, #8453) carrying either shRNA sequences targeting NCKAP1 (sh-NCKAP1, 5'-CCGG AACATCTACAAATGTGAAGTACTCGAG CTTCACATTTGTAGATGTTATTTTTT-3') or the scrambled (sh-NC, 5'-CCGGCAACAAGATGAAGAGCACC AACTCGAGTTGGTGCTCTTCATCTTGTTGTTTTT -3'). HEK293T packaging cells (CL-0005, Procell Life Science & Technology, Wuhan, China) were maintained in high-glucose DMEM with 10% FBS and 1% P/S. The cell line was authenticated by short tandem repeat (STR) profiling and tested negative for mycoplasma contamination. Viral particles were produced by co-transfecting pLKO.1 with psPAX2 (Addgene, #12260) and pMD2.G (Addgene, #12259) using Lipofectamine 3000. Viral supernatants collected at 48 and 72 h were combined, passed through 0.45-µm polyethersulfone filters (Millipore, Burlington, MA, USA, #SLHP033RS), and applied to SCC-9 cells in the presence of 8 µg/mL polybrene (Sigma-Aldrich, St. Louis, MO, USA, #TR-1003). Puromycin selection (2 µg/mL; Gibco, Thermo Fisher Scientific, Grand Island, NY, USA, #A1113803) was continued for 7 days, after which NCKAP1 depletion was verified by Western blotting.

Cell Viability Assay (CCK-8)

Cells were plated at 5000 cells per well in 96-well plates and allowed to attach overnight. Following treatment, 10 µL of CCK-8 reagent (Dojindo Laboratories, Kumamoto, Japan, #CK04) was added, and the plates were incubated for 2 h at 37 °C before absorbance was measured at 450 nm with a SpectraMax M5 microplate reader (Molecular Devices). Cell viability was expressed as a percentage of the corresponding control condition. In experiments involving DTT or TCEP, cells in all experimental conditions were gently washed twice with pre-warmed PBS, and the medium was replaced with reducing-agent-free medium to remove residual reducing agents that could directly reduce the WST-8 dye.

LDH Release Assay

Membrane damage was quantified using the CytoTox-ONE Homogeneous Membrane Integrity Assay (Promega, Madison, WI, USA, #G7891). A 50-µL aliquot of culture supernatant was mixed with the assay substrate in a 96-well plate and incubated for 10 min at room temperature in the dark. Fluorescence was measured at an excitation wavelength of 560 nm, and LDH release was calculated relative to parallel wells lysed with 1% Triton X-100.

Annexin V/PI Flow Cytometry

Annexin V/PI staining was performed with the Annexin V-FITC/PI Apoptosis Detection Kit (BD Biosciences, Franklin Lakes, NJ, USA, #556547). Adherent and floating cells were pooled after EDTA-free trypsinization (Gibco, Thermo Fisher Scientific, Grand Island, NY, USA, #15050065), washed twice in cold PBS, and suspended in 100 µL binding buffer. Each sample was stained with 5 µL Annexin V-FITC and 5 µL propidium iodide for 15 min at room temperature in the dark, diluted with another 400 µL of binding buffer, and analyzed on a FACSCanto II flow cytometer (BD Biosciences, San Jose, CA, USA). At least 10000 events were collected per sample and analyzed using FlowJo v10.8 (FlowJo LLC, BD Biosciences, Ashland, OR, USA).

DTNB Assay for Total Free Thiol Content

Total intracellular free thiols were assessed using the DTNB-based Total Thiol Assay Kit (Beyotime, Shanghai, China, #S0141). After treatment, cells were rinsed three times with ice-cold PBS to remove residual extracellular reducing agents and lysed in the supplied buffer for 30 min on ice. Cleared lysates were obtained by centrifugation at 12,000 ×g for 10 min at 4 °C, and protein concentrations were determined using the BCA assay (Pierce, Thermo Fisher Scientific, Rockford, IL, USA, #23225). Protein samples (20 µg) were reacted with DTNB working solution for 5 min at 37 °C, and absorbance was measured at 412 nm using a SpectraMax M5 reader (Molecular Devices, San

Jose, CA, USA). Free thiol content was expressed either as a percentage of the control condition (Fig. 3A, Fig. 4G,H) or as nmol thiol per mg protein (Fig. 5C), as indicated in the figure legends.

NADPH/NADP$^+$ Ratio Measurement

The intracellular NADPH/NADP$^+$ ratio was measured using the NADP/NADPH Quantitation Colorimetric Kit (BioVision, Waltham, MA, USA, #K347-100). Lysates were prepared in the kit extraction buffer. To quantify NADPH alone, one aliquot was heated at 60 °C for 30 min to degrade NADP$^+$, while an unheated aliquot was used to determine total NADP (NADPH + NADP$^+$). Both extracts were incubated with the NADP cycling enzyme mix and chromogenic substrate, and absorbance was measured at 450 nm. NADPH and NADP$^+$ concentrations were calculated against a freshly prepared NADPH standard curve, and the NADPH/NADP$^+$ ratio was derived as the absolute ratio of the two values.

Intracellular Glutathione (Total Glutathione, GSSG, GSH and GSH/GSSG Ratio) Measurement

Total glutathione, oxidized glutathione (GSSG) and reduced glutathione (GSH) were quantified using the GSH and GSSG Assay Kit (Beyotime, Shanghai, China, #S0053), which is based on the DTNB-glutathione reductase recycling reaction. After treatment, cells were rinsed three times with ice-cold PBS, harvested, deproteinized with 5% metaphosphoric acid (Sigma-Aldrich, St. Louis, MO, USA, #239275) and centrifuged at 12,000 ×g for 10 min at 4 °C. Each supernatant was divided into two aliquots. In the first aliquot, total glutathione was determined directly. The sample was mixed with DTNB and glutathione reductase in the presence of NADPH, and absorbance at 412 nm was recorded every minute for 5 min. The rate of TNB formation was converted to concentration using a freshly prepared GSSG standard curve processed in parallel under identical conditions. Because the recycling reaction detects GSH and GSSG-derived GSH equivalently, this value represents total glutathione expressed as GSH equivalents, that is GSH + 2 × GSSG. In the second aliquot, reduced GSH was first masked using the GSH-scavenging reagent supplied with the kit for 60 min at 25 °C according to the manufacturer's instructions, allowing only GSSG to enter the subsequent recycling reaction. GSSG was then measured using the same procedure and standard curve. Reduced GSH was calculated by subtraction as GSH = total glutathione – 2 × GSSG, and the cellular redox state was expressed as the GSH/GSSG molar ratio, which more accurately reflects thiol redox balance than reduced GSH alone. In each independent experiment, GSH and GSSG standards of known concentrations were subjected to the masking step in parallel with the samples. The masked GSH standard produced a signal below 3% of that of the unmasked standard, and GSSG recovery was within 95–105% of the nominal value. All values were normalized to the protein concentration of a matched, non-deproteinized lysate determined by BCA assay (Pierce, Thermo Fisher Scientific, Rockford, IL, USA, #23225) and are reported as nmol per mg protein.

Quantitative Reverse-Transcription PCR (qRT-PCR)

RNA was extracted using TRIzol (Invitrogen, Waltham, MA, USA, #15596018), and RNA integrity was assessed by 1% agarose gel electrophoresis. RNA (1 µg) was reverse transcribed using the PrimeScript RT Reagent Kit with gDNA Eraser (TakaraBio, Kusatsu, Shiga, Japan, #RR047A). Quantitative PCR was performed on a QuantStudio 3 PCR system (Applied Biosystems, Thermo Fisher Scientific, Waltham, MA, USA) using TB Green Premix Ex Taq II (Takara, #RR820A), and relative expression levels were calculated using the $2^{-\Delta\Delta Ct}$ method. Because GAPDH is a glycolytic enzyme, it was used as the reference gene only for comparisons among glucose-replete samples (cell-line expression profiling and validation of knockdown/overexpression). No qRT-PCR quantification was performed across conditions with differing glucose availability or metabolic states. Primer sequences are provided in Table 1.

Western Blot

RIPA buffer (Beyotime, Shanghai, China, #P0013B) containing protease (RocheDiagnostics, Mannheim, Germany, #04693132001) and phosphatase (Roche, #04906837001) inhibitor cocktail was used for protein extraction. Lysates were incubated on ice for 30 min with periodic mixing and clarified by centrifugation at 12,000 ×g for 15 min at 4 °C. Following BCA quantification, 30 µg of protein per lane was resolved on 8–10% SDS-PAGE and transferred to PVDF membranes (Millipore, Burlington, MA, USA, #IPVH00010) at 100 V for 90 min at 4 °C. Membranes were blocked with 5% non-fat milk in TBST for 1 h at room temperature and incubated overnight at 4 °C with primary antibodies (NCKAP1, 1:1000, A12229, Abclonal Technology, Wuhan, China; SLC7A11, 1:1000, HA721868, HUABIO, Woburn, MA, USA; GAPDH, 1:5000, 60004-1-Ig, Proteintech, Rosemont, IL, USA). After three washes in TBST, membranes were incubated with HRP-conjugated secondary antibody (1:2000, ZB2301/2305, ZS Golden Bridge, Beijing, China) for 1 h at room temperature. Protein bands were visualized using enhanced chemiluminescence reagent (Millipore, #WBKLS0500) and imaged with a ChemiDoc MP system (Bio-Rad Laboratories, Hercules, CA, USA). Band intensities were quantified using Fiji/ImageJ v2.9.0 (National Institutes of Health, Bethesda, MD, USA). GAPDH was used as a loading control only for comparisons among glucose-replete samples (Fig. 1 and Fig. 4B,D). No Western-blot quantification was normalized to GAPDH across conditions with differing metabolic states.

Table 1. Primer sequences.

Name	Forward (5'-3')	Reverse (5'-3')
NCKAP1	CAACATCAAGAAGGCATGTGGA	TAGTTGTGCAAGCTGTTGATTGTT
SLC7A11	ATCTGCCCAAGGGGAGACAC	TTTGAAGGTTCTTTGCCGTGC
GAPDH	TTTTGCGTCGCCAGCC	ATGGAATTTGCCATGGGTGGA

Colony Formation Assay

Stable sh-NC or sh-NCKAP1 SCC-9 cells were seeded into 6-well plates at 500 cells per well in complete medium for 14 days, with medium replaced every 3 days. Colonies were fixed in 4% paraformaldehyde for 15 min, stained for 20 min using 0.1% crystal violet (Sigma-Aldrich, St. Louis, MO, USA, #C0775), washed, and air-dried. Whole wells were scanned with an Epson Perfection V850 (Seiko Epson Corporation, Suwa, Nagano, Japan). Colonies containing ≥50 cells were enumerated manually by an investigator blinded to group allocation.

Wound Healing Assay

Confluent monolayers (approximately 90%) in 6-well plates were scratched with a sterile 200 µL pipette tip held perpendicular to the plate. After two PBS washes to remove detached material, cells were maintained in serum-free medium to limit proliferation related closure. Reference marks on the bottom of each well allowed the same field to be imaged at 0 and 24 h using an Olympus IX73 inverted phase-contrast microscope. Wound area was measured in Fiji/ImageJ v2.9.0 (National Institutes of Health, Bethesda, MD, USA), and closure was calculated as Wound closure (%) = 100% × (A0-At)/A0, where A0 and At denote the wound areas at baseline and time t, respectively.

Transwell Migration Assay

Migration was tested in 24-well Transwell inserts fitted with 8 µm polycarbonate membranes (Corning Incorporated, Corning, NY, USA, #3422). After 6 h of serum deprivation, 5×10^4 cells in 200 µL serum-free medium were loaded into the upper chamber, and 600 µL complete medium containing 20% FBS was placed below as the chemoattractant. After 24 h at 37 °C, cells remaining on the upper membrane were removed with a cotton swab. Cells that had crossed to the lower surface were fixed in 4% paraformaldehyde for 15 min, stained with 0.1% crystal violet for 20 min, washed, and dried. Five random fields per insert were imaged at 200× magnification, and migrated cells were counted using Fiji/ImageJ v2.9.0.

Statistical Analysis

All quantitative data are presented as mean ± standard deviation (SD) from five independent biological experiments. Throughout, n indicates the number of independent biological experiments. For all image-based quantification, measurements from multiple cells or fields within each experiment were averaged to generate a single value per experiment before statistical analysis, ensuring that the biological replicate, rather than the individual cells or fields, served as the statistical unit. Statistical analyses were performed using GraphPad Prism v10.1.2 (GraphPad Software, San Diego, CA, USA). Before comparisons, the distribution of each continuous variable was assessed for normality using the Shapiro-Wilk test, and homogeneity of variance was evaluated using the F-test (two groups) or Brown-Forsythe test (three or more groups). All datasets met both assumptions (Shapiro-Wilk $p > 0.05$ for all groups), and parametric tests were therefore applied. Comparisons between two groups were performed using a two-tailed unpaired Student's *t*-test. Comparisons among three or more groups were performed using one-way ANOVA followed by Tukey's post-hoc test. For the four GF-treated genetic backgrounds compared in Fig. 6F–J, two pre-planned comparisons(si-NCKAP1 versus si-NC and OE-NCKAP1 versus OE-NC) were evaluated within the same one-way ANOVA framework with Tukey's correction. Experiments involving two crossed factors were analyzed using two-way ANOVA followed by Tukey's multiple-comparisons correction. If normality had not been satisfied, the Mann-Whitney U test (two groups) or Kruskal-Wallis test with Dunn's post-hoc test would have been applied. If variances had been unequal, Welch's correction would have been used. A two-sided p value < 0.05 was considered statistically significant.

Results

NCKAP1 and SLC7A11 Were Higher in Two OSCC Cell Lines Than in HOK Cells Under Their Respective Routine Culture Conditions

To determine whether OSCC cells possess the molecular background associated with disulfide stress-associated cell death, we first examined the expression of NCKAP1 and SLC7A11 in two OSCC cell lines and in normal human oral keratinocytes (HOK). Each line was maintained in its own routine culture medium, so that the comparison is between cells under their respective routine culture conditions rather than in a common medium. qRT-PCR analysis showed that NCKAP1 and SLC7A11 mRNA expression levels were higher in SCC-9 and CAL-27 cells than in HOK cells (Fig. 1A,B, $p < 0.001$). Western blot analysis confirmed higher protein expression of both NCKAP1 and SLC7A11 in OSCC cells than in normal oral keratinocytes (Fig. 1C–E, $p < 0.001$). Among the two OSCC cell lines,

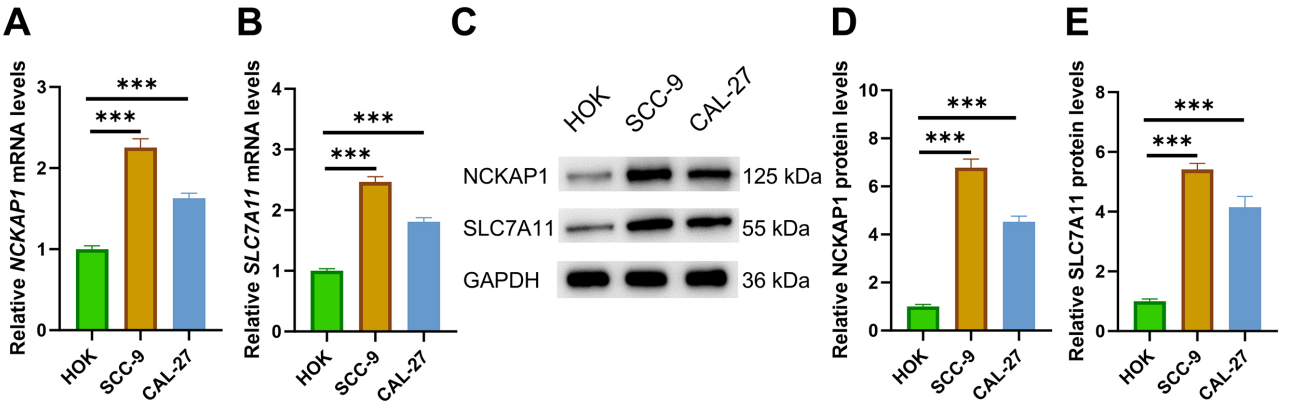

Fig. 1. NCKAP1 and SLC7A11 were higher in two OSCC cell lines than in HOK cells under their respective routine culture conditions. (A,B) Relative mRNA expression of NCKAP1 (A) and SLC7A11 (B) measured by qRT-PCR. (C) Representative Western blot of NCKAP1, SLC7A11 and GAPDH in HOK, SCC-9 and CAL-27 cells. (D,E) Quantification of NCKAP1 (D) and SLC7A11 (E) protein levels normalized to GAPDH. Each cell line was maintained in its own routine medium; the comparison is therefore not matched for culture conditions. Data are mean ± SD, from n = 5 independent biological replicates. *** $p < 0.001$. HOK, human oral keratinocytes; OSCC, oral squamous cell carcinoma.

SCC-9 cells showed relatively higher expression of both proteins and were therefore selected as the major cell model for subsequent mechanistic experiments.

Glucose Starvation Triggered a Non-Apoptotic, Disulfide Stress-Driven Cell Death in SCC-9 Cells

Disulfidptosis is precipitated by glucose-starvation-induced NADPH depletion in SLC7A11-high cells. We first assessed whether transfer to glucose-free culture conditions was sufficient to induce cell death in SCC-9 cells. SCC-9 cells were switched to glucose-free DMEM supplemented with 10% dialyzed FBS. CCK-8 assays revealed a time-dependent decline in cell viability (Fig. 2A, all $p < 0.001$), accompanied by increased LDH release into the medium (Fig. 2B, all $p < 0.001$). Phase-contrast microscopy showed that glucose-deprived cells progressively developed a rounded, balloon-like morphology and rapidly detached from the substrate (Fig. 2C), features previously described in disulfidptosis [16,17]. Annexin V/PI flow cytometry demonstrated that 4 h of glucose starvation reduced the viable cell fraction (AV^-/PI^-, $p < 0.001$) and predominantly increased the PI-single-positive necrotic fraction (AV^-/PI^+, $p < 0.001$), with a smaller increase in the double-positive late-apoptotic fraction (AV^+/PI^+, $p < 0.001$). In contrast, the Annexin V-single-positive early-apoptotic fraction (AV^+/PI^-) remained minimal ($p < 0.001$). Thus, the dying population was predominantly PI-single-positive rather than Annexin V-positive, arguing against classical apoptosis (Fig. 2D,E).

To assess the contribution of established death modalities, cells were treated with pathway-specific inhibitors during 4 h of glucose starvation. As shown in Fig. 2F, Z-VAD-FMK (20 μM, pan-caspase), Necrostatin-1 (20 μM, RIPK1), 3-MA (5 mM, autophagy) and Ferrostatin-1 (2 μM, lipid peroxidation) failed to rescue cell viability under the tested conditions ($p > 0.05$). In contrast, co-treatment with the disulfide-reducing agent DTT (1 mM) preserved cell viability ($p < 0.001$). Because DTT was present from the onset of glucose starvation, these findings indicate that the death process requires a thiol-reducible component, although they do not by themselves establish the location of this process. Together with the predominantly PI-single-positive staining pattern and rescue by disulfide-reducing agents, these data are most consistent with disulfide stress-driven cell death rather than apoptosis, necroptosis, autophagy-dependent cell death, or ferroptosis, while not formally excluding contributions from these pathways.

A Thiol-Reducible Process was Required for Cell Death During Glucose Starvation

To assess the cellular redox state in our model, we quantified total intracellular free thiols as a bulk indicator of thiol oxidation. Glucose starvation for 4 h markedly reduced free thiol content ($p < 0.001$), consistent with extensive disulfide-bond formation. Co-treatment with the reducing agents DTT (1 mM) or TCEP (500 μM) restored free thiols to 85.9% and 81.3% of the control level, respectively, a substantial but incomplete recovery that remained significantly below the controls (Fig. 3A, $p < 0.001$ vs GF for both; $p < 0.01$ and $p < 0.001$ vs Ctrl, respectively).

CCK-8 assays confirmed that both reducing agents substantially, but incompletely, restored cell viability during glucose starvation, to 78.2% and 72.5% of control for DTT and TCEP respectively (Fig. 3B, $p < 0.001$ vs GF and vs Ctrl). Neither compound exerted cytotoxicity in the absence of glucose stress: DTT or TCEP alone did not reduce viability relative to untreated control (95.7% and 95.4% of control, respectively; $p > 0.05$ vs Ctrl), and

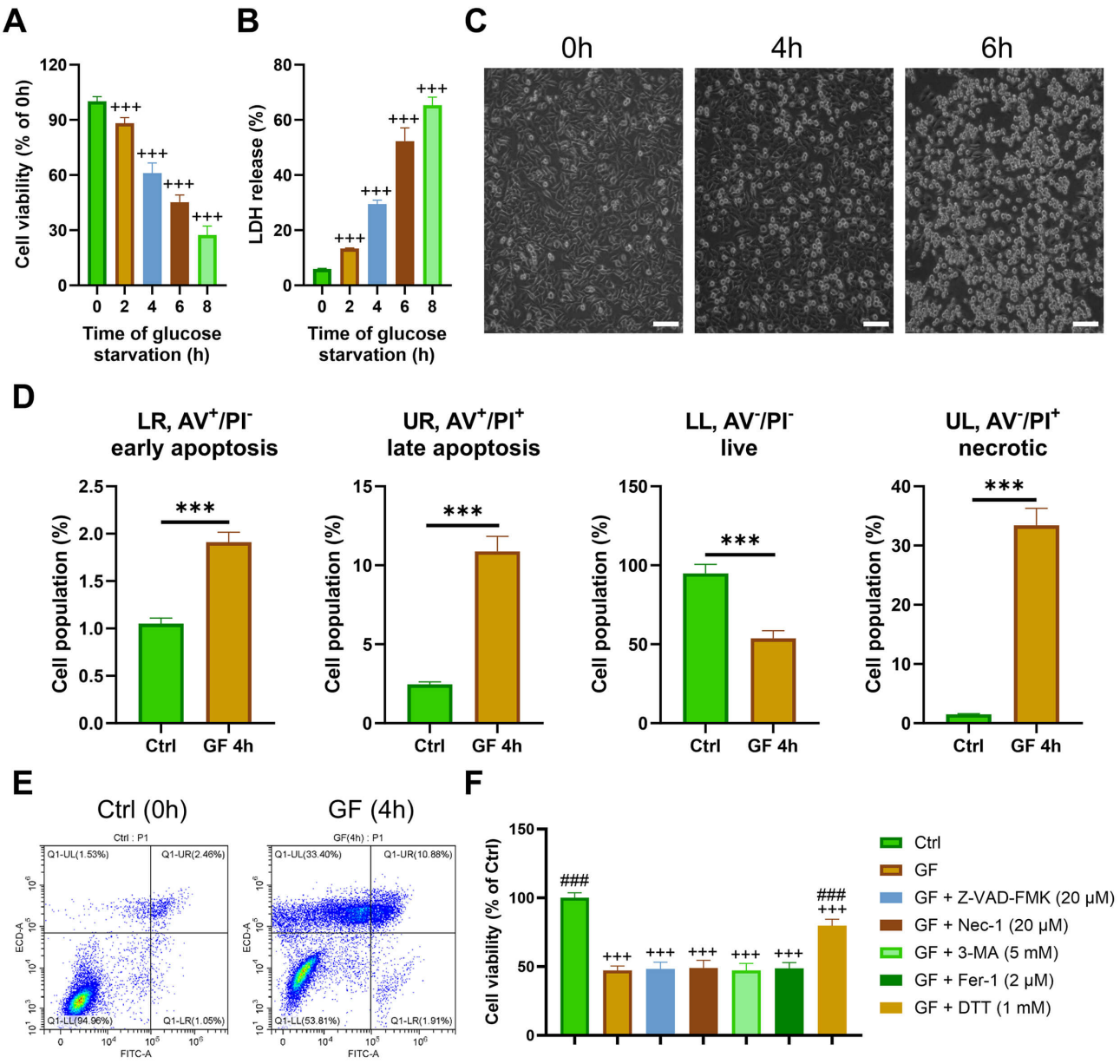

Fig. 2. Glucose starvation induced a non-apoptotic, disulfide stress-driven cell death in SCC-9 cells. (A) Cell viability assessed by CCK-8 over 0–8 h of glucose starvation (GF). (B) Corresponding LDH release into the culture supernatant. (C) Representative phase-contrast images at 0, 4 and 6 h (scale bar: 100 μm). (D) Quantification of cell death subpopulations. (E) Representative Annexin V-FITC/PI flow cytometry dot plots after 4 h GF. (F) CCK-8 viability of SCC-9 cells after 4 h GF in the presence of Z-VAD-FMK, Necrostatin-1, 3-MA, Ferrostatin-1 or DTT. Data are mean ± SD (n = 5). +++ $p < 0.001$ vs. Ctrl (0 h GF). ### $p < 0.001$ vs. GF. *** $p < 0.001$.

both differed significantly from the GF group ($p < 0.001$). To exclude direct chemical reduction of the WST-8 dye by the reducing agents, viability measurements were performed after washing out DTT/TCEP and replacing the medium with reducing-agent-free medium. The rescue by DTT and TCEP was preserved, indicating genuine preservation of cell viability rather than a dye artifact. Together, the biochemical (DTNB) and functional (CCK-8) readouts changed in a mutually consistent manner, indicating that a thiol-reducible process is required for cell death in glucose-starved SCC-9 cells. The rescue afforded by both agents was consistently partial across the biochemical and functional readouts, indicating that reduction of disulfide stress attenuates but does not fully abolish the consequences of glucose-free culture. We emphasize that the reducing agents were present from the onset of starvation and also reduce extracellular cystine to cysteine, which can be imported independently of SLC7A11. These experiments

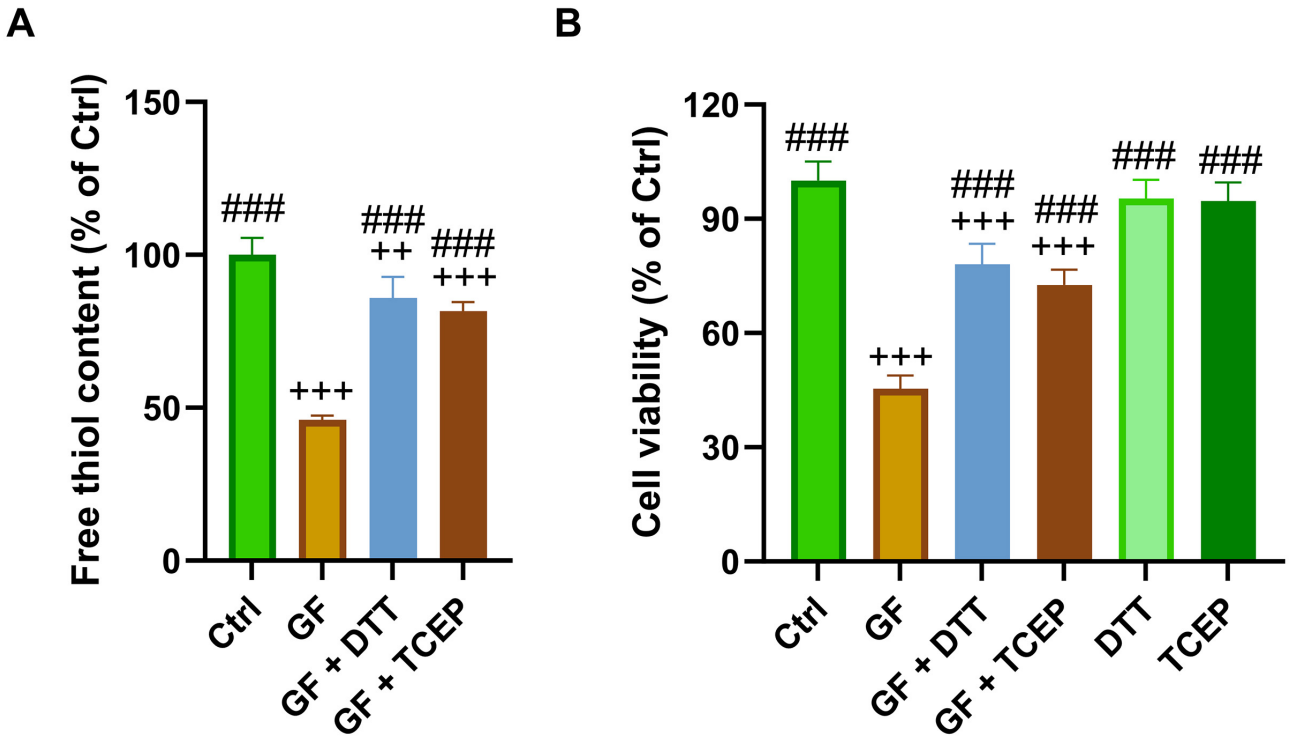

Fig. 3. A thiol-reducible process was required for cell death in glucose-starved SCC-9 cells. (A) Intracellular free-thiol content of SCC-9 cells measured by DTNB after 4 h of treatment with control medium, glucose-free medium (GF), GF + DTT (1 mM) or GF + TCEP (500 µM). (B) CCK-8 cell viability, including DTT-alone and TCEP-alone controls. Data are mean ± SD (n = 5). ++ $p < 0.01$, +++ $p < 0.001$ vs Ctrl. ### $p < 0.001$ vs GF. All pairwise comparisons were made by one-way ANOVA followed by Tukey's post-hoc test. Groups without a symbol did not differ significantly from the indicated reference group.

therefore do not establish that the relevant reduction occurs intracellularly, nor that thiol oxidation is the proximate trigger.

NCKAP1 Levels Bidirectionally Determined Cell Viability and Free-thiol Depletion Under Glucose Starvation in SCC-9 Cells

NCKAP1, as a structural component of the WAVE regulatory complex, links upstream Rac1 signaling to Arp2/3-driven actin branching. We therefore tested whether NCKAP1 levels causally determine the extent of the viability loss produced by glucose starvation. SCC-9 cells were transfected with NCKAP1 siRNA (si-NCKAP1) or a control siRNA (si-NC), achieving efficient knockdown at the mRNA and protein levels (Fig. 4A,B, $p < 0.001$). Conversely, transient transfection of a Flag-NCKAP1 plasmid produced robust overexpression at both mRNA and protein levels compared with empty vector (OE-NC) (Fig. 4C,D, $p < 0.001$).

After 4 h of glucose starvation, NCKAP1 silencing markedly preserved cell viability, while having no detectable effect on viability under basal conditions (Fig. 4E, $p < 0.001$). Conversely, NCKAP1 overexpression further reduced viability under glucose starvation (Fig. 4F, $p < 0.001$). Importantly, DTNB analysis showed that NCKAP1 knockdown partially restored free-thiol content under GF, whereas NCKAP1 overexpression aggravated thiol depletion (Fig. 4G,H, all $p < 0.001$), indicating that NCKAP1 levels are associated with the extent of net free-thiol loss under glucose starvation.

The Contribution of NCKAP1 Is Conditional on SLC7A11-Mediated Cystine Import

To determine whether the contribution of NCKAP1 depends on SLC7A11-mediated cystine import in this disulfide stress-driven cell death, we generated four genetic conditions in SCC-9 cells (si-NC, si-SLC7A11, si-NCKAP1, and si-SLC7A11 + OE-NCKAP1). SLC7A11 silencing significantly reduced SLC7A11 mRNA expression ($p < 0.001$, Fig. 5A).

All four genetic combinations were subjected to 4 h of glucose starvation. SLC7A11 silencing almost completely prevented GF-induced loss of viability, with values comparable to non-starved controls, indicating that cystine import via SLC7A11 is required for this process (Fig. 5B, $p < 0.001$). NCKAP1 silencing afforded substantial but partial protection. In cells in which SLC7A11 had been silenced, additional transfection of the NCKAP1 plasmid failed to reduce viability (ns versus si-SLC7A11 + GF). This observation is consistent with a functional dependency, in which the

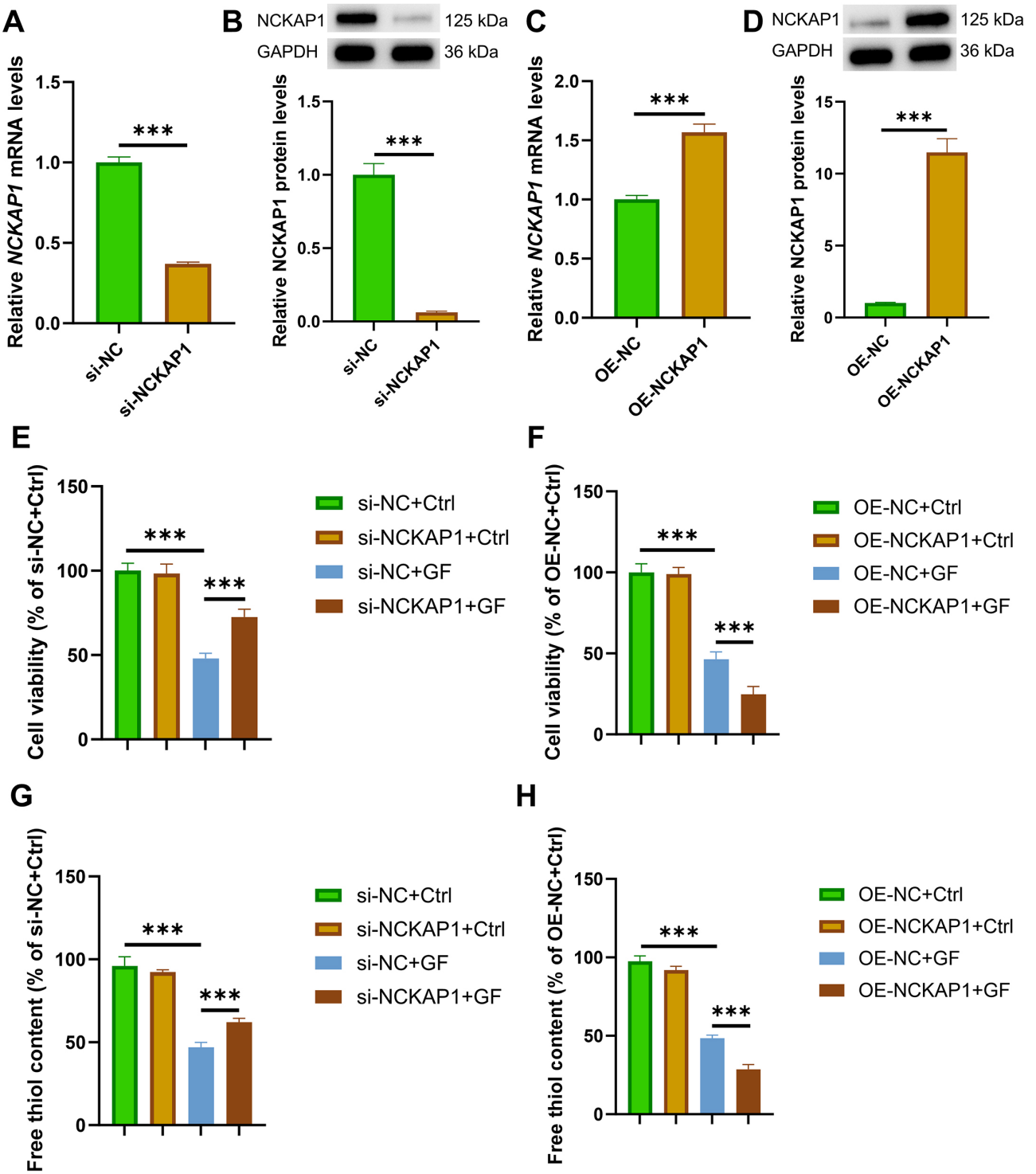

Fig. 4. NCKAP1 expression bidirectionally determined the loss of cell viability and free-thiol depletion under glucose starvation in SCC-9 cells. (A) qRT-PCR validation of NCKAP1 knockdown by siRNA. (B) Western-blot validation of NCKAP1 knockdown. (C) qRT-PCR validation of Flag-NCKAP1 overexpression. (D) Western-blot validation of NCKAP1 overexpression. (E) CCK-8 viability of si-NC and si-NCKAP1 cells under control or GF (4 h) conditions. (F) CCK-8 viability of OE-NC and OE-NCKAP1 cells under control or GF conditions. (G) DTNB free-thiol content in the knockdown groups. (H) DTNB free-thiol content in the overexpression groups. Data are mean ± SD (n = 5). *** $p < 0.001$.

contribution of NCKAP1 requires SLC7A11-mediated cystine import. It should be noted, however, that a si-SLC7A11 group transfected with the empty vector was not included and that the two manipulations were not verified simultane-

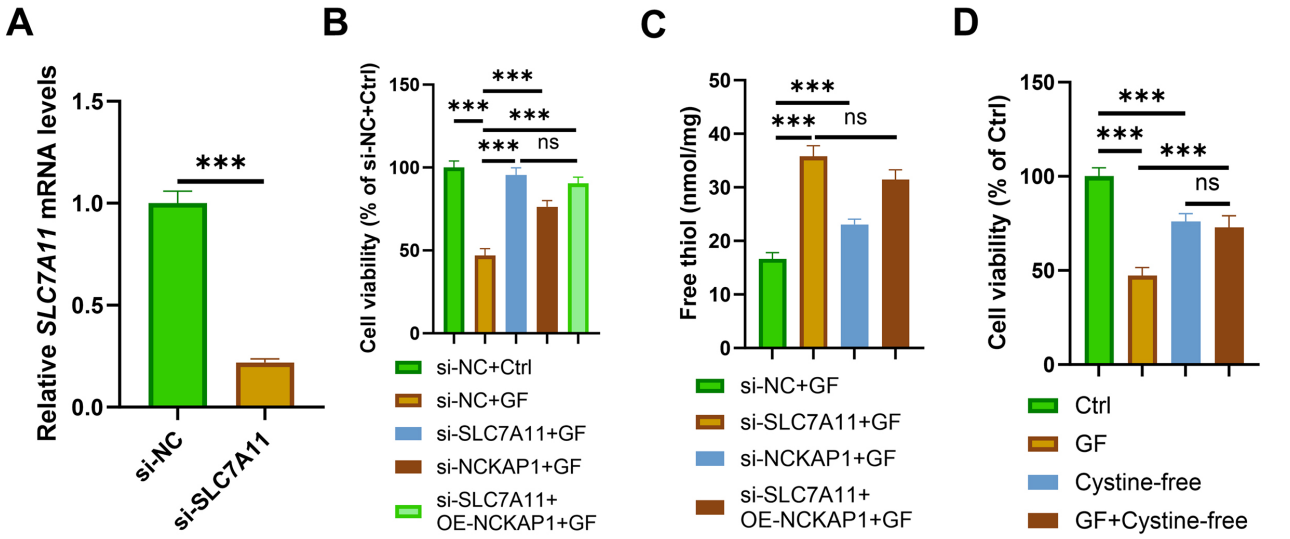

Fig. 5. The effect of NCKAP1 on cell viability under glucose starvation is conditional on SLC7A11-mediated cystine import. (A) Validation of SLC7A11 knockdown. Relative SLC7A11 mRNA levels measured by qRT-PCR in si-SLC7A11 versus si-NC cells. (B) CCK-8 viability. (C) DTNB free-thiol content (expressed as absolute concentration, nmol/mg protein). (D) CCK-8 viability under cystine-free and GF+ cystine-free conditions. The si-SLC7A11 + OE-NCKAP1 group was compared with si-SLC7A11 alone. A si-SLC7A11 + empty-vector group was not included, and knockdown of SLC7A11 and overexpression of NCKAP1 were verified in separate transfections (Fig. 4B,D, Fig. 5A) rather than simultaneously in the dual-transfected population. Data are mean ± SD (n = 5). ns, not significant. *** $p < 0.001$.

ously in the dual-transfected cells, so that this experiment cannot establish a formal linear upstream–downstream relationship. DTNB free-thiol measurements followed the same trend (Fig. 5C): si-SLC7A11 groups displayed near-baseline thiol levels regardless of NCKAP1 status, whereas si-NCKAP1 partially preserved thiol levels compared with si-NC + GF (all $p < 0.001$).

Replacing the medium with cystine-free DMEM induced only modest loss of viability, whereas combining cystine-free conditions with glucose starvation (GF + Cystine-free) significantly attenuated the canonical GF phenotype (Fig. 5D, all $p < 0.001$), indicating that cystine influx is a prerequisite for full execution of this death process. Having established that SLC7A11-mediated cystine import is required for this process and that increasing NCKAP1 does not compensate for its loss, we next examined the metabolic module in detail and asked whether NCKAP1 acts within it.

Glucose Starvation Depleted and Oxidized the Glutathione Pool, Whereas NCKAP1 Manipulation Had Only Marginal Effects on this Metabolic Module

Because the GSH/GSSG ratio reflects cellular redox state more faithfully than reduced GSH alone, we resolved the glutathione pool into its individual components rather than reporting a single recycling-assay value. Glucose starvation produced a rapid fall in the NADPH/$NADP^+$ ratio, which declined to 0.42-fold of baseline by 4 h and to 0.31-fold by 6 h (Fig. 6A, all $p < 0.001$ vs 0 h). In parallel, the total glutathione pool was progressively depleted, from 34.6 nmol/mg protein at baseline to 15.3 nmol/mg at 4 h and 13.2 nmol/mg at 6 h (Fig. 6B, all $p < 0.001$). This depletion was accompanied by a concomitant accumulation of GSSG, which rose from 0.79 to 2.45 nmol/mg at 4 h and to 2.77 nmol/mg at 6 h (Fig. 6C, all $p < 0.001$), and by a steeper loss of reduced GSH, from 33.2 to 10.7 nmol/mg at 4 h and 7.6 nmol/mg at 6 h (Fig. 6D, all $p < 0.001$). Consequently, the GSH/GSSG ratio collapsed from 40.1 at baseline to 4.5 at 4 h and 2.7 at 6 h, corresponding to decreases of approximately 89% and 93%, respectively (Fig. 6E, all $p < 0.001$). Glucose starvation therefore not only depleted glutathione but also shifted the surviving pool decisively toward the oxidized state. Together with the loss of NADPH, these changes provide a metabolic context favoring disulfide-bond formation.

We next asked whether NCKAP1 acts within this metabolic module. Because all four genetic backgrounds (si-NC, si-NCKAP1, OE-NC and OE-NCKAP1) received the same 4 h of glucose starvation, glutathione parameters are reported as absolute values (nmol/mg protein) to allow direct comparison of the metabolic state, whereas the NADPH/$NADP^+$ ratio is expressed relative to si-NC + GF. The size of the glutathione pool and the amount of oxidized glutathione were unaffected by NCKAP1 manipulation. Neither total glutathione (Fig. 6G) nor GSSG content (Fig. 6H) differed between si-NCKAP1 and si-NC or between OE-NCKAP1 and OE-NC (all $p > 0.05$). Reduced GSH and the GSH/GSSG ratio did show small but statis-

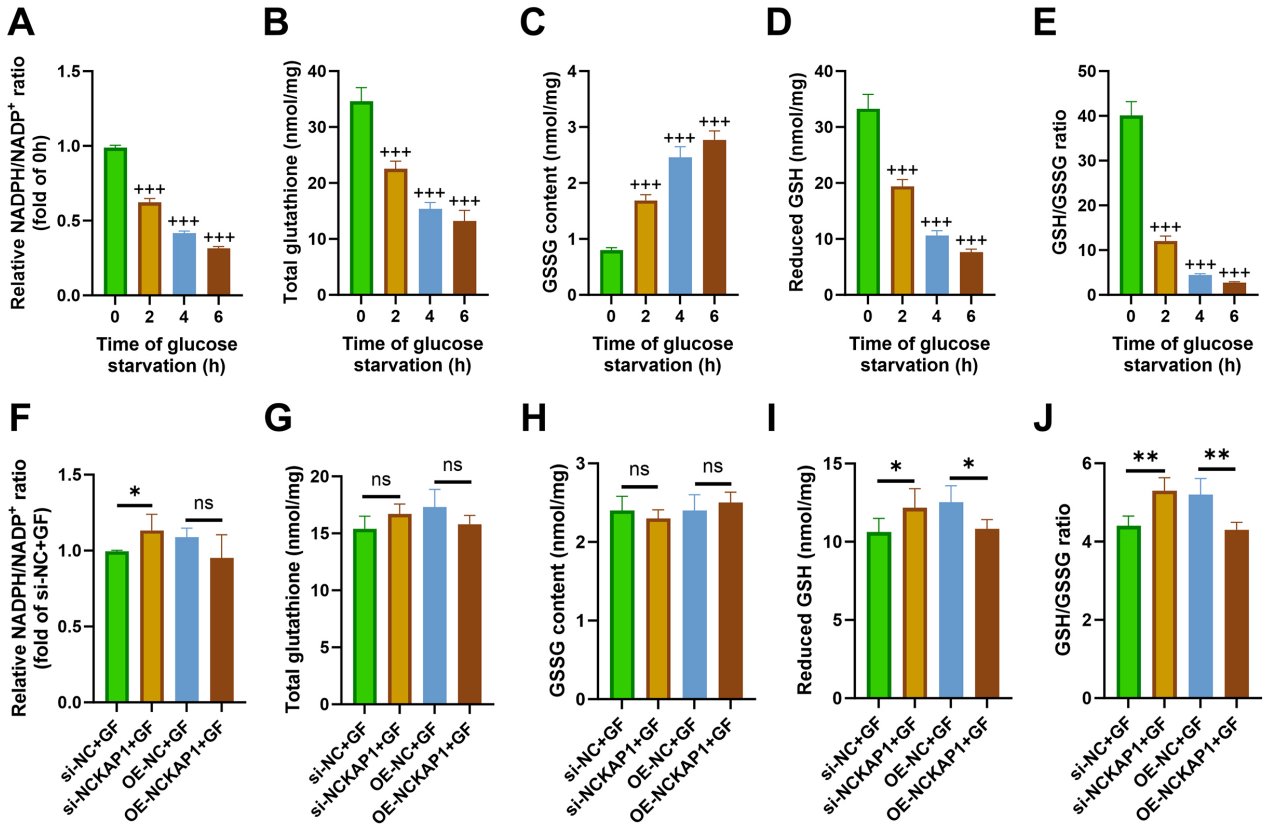

Fig. 6. Glucose starvation depleted and oxidized the glutathione pool, whereas NCKAP1 manipulation had only marginal effects on this metabolic module. (A–E) SCC-9 cells were subjected to glucose starvation (GF) for 0, 2, 4 and 6 h. (A) Relative NADPH/NADP$^+$ ratio (fold of 0 h). (B) Total glutathione, determined by the DTNB–glutathione reductase recycling assay and expressed in GSH equivalents (GSH + 2 × GSSG). (C) GSSG content, measured after masking of reduced GSH. (D) Reduced GSH, calculated as total glutathione – 2 × GSSG. (E) GSH/GSSG molar ratio. (F–J) si-NC, si-NCKAP1, OE-NC and OE-NCKAP1 SCC-9 cells were all subjected to 4 h of GF and the same five parameters were determined. (F) relative NADPH/NADP$^+$ ratio (fold of si-NC + GF), (G) total glutathione, (H) GSSG content, (I) reduced GSH and (J) GSH/GSSG ratio. Because every group received GF, glutathione parameters are shown as absolute values (nmol/mg protein) to allow direct comparison of the metabolic state. Data are mean ± SD (n = 5). +++ $p < 0.001$ vs 0 h. * $p < 0.05$, ** $p < 0.01$, ns, not significant. All comparisons were made by one-way ANOVA followed by Tukey's post-hoc test.

tically significant shifts in the direction predicted by the viability phenotype. NCKAP1 knockdown raised reduced GSH from 10.6 to 12.2 nmol/mg (Fig. 6I, $p < 0.05$) and the GSH/GSSG ratio from 4.4 to 5.3 (Fig. 6J, $p < 0.01$), whereas NCKAP1 overexpression produced the converse changes, from 12.5 to 10.8 nmol/mg ($p < 0.05$) and from 5.2 to 4.3 ($p < 0.01$), respectively. The NADPH/NADP$^+$ ratio was marginally higher in si-NCKAP1 cells (Fig. 6F, $p < 0.05$) and was not significantly altered by NCKAP1 overexpression ($p > 0.05$).

These differences were an order of magnitude smaller than the starvation-induced changes themselves. Relative to the time course in Fig. 6A–E, in which si-NC + GF at 4 h (reduced GSH 10.6 nmol/mg, GSH/GSSG 4.4) closely reproduced the corresponding 4 h time point (10.7 nmol/mg, 4.5), NCKAP1 knockdown recovered only about 2.5% of the starvation-induced fall in the GSH/GSSG ratio, about 7% of the fall in reduced GSH, and about 9% of the fall in the NADPH/NADP$^+$ ratio. NCKAP1 was therefore neither able to prevent nor required for the metabolic collapse that preceded disulfide stress. The small residual differences may reflect a consequence of the viability phenotype rather than an action of NCKAP1 within the NADPH-glutathione module, since cells with a less elaborate branched-actin network would be expected to present fewer oxidizable thiols and consume fewer reducing equivalents. Consistent with this, the increment in total free thiols conferred by NCKAP1 knockdown under starvation (16.5 to 23.0 nmol/mg, Fig. 5C) was approximately fourfold larger than the accompanying increment in reduced GSH (1.6 nmol/mg), indicating that most of the preserved thiol pool was non-glutathione and likely protein-associated. These observations argue against a major role of NCKAP1 in the redox collapse itself and are consistent with a role for NCKAP1 in WAVE-complex-associated cytoskeletal regulation, which was not examined directly here. We note, however, that this in-

ference rests on the small magnitude of the metabolic effect and on a failure to rescue; a minor contribution of NCKAP1 to redox homeostasis therefore cannot be formally excluded, and a strictly linear upstream–downstream relationship cannot be established from these experiments alone.

NCKAP1 Knockdown Suppressed OSCC Proliferation and Migration

Beyond its role in this death process, NCKAP1 governs actin branching in lamellipodia and may therefore contribute to OSCC malignant behavior under nutrient-replete conditions. To address this, we generated SCC-9 stable lines expressing sh-NCKAP1 or sh-NC by lentiviral transduction and puromycin selection. Western blot confirmed robust knockdown of NCKAP1 protein in the stable knockdown line (Fig. 7A, $p < 0.001$). Colony-formation assays revealed that sh-NCKAP1 cells produced markedly fewer and visibly smaller colonies than sh-NC controls (Fig. 7B,C, $p < 0.001$). Wound-healing assays showed substantially delayed gap closure at both 24 h (Fig. 7D,E, $p < 0.001$), and Transwell migration assays confirmed the deficit (Fig. 7F,G, $p < 0.001$). These *in vitro* findings are consistent with a dual role for NCKAP1 in this OSCC cell model. NCKAP1 supports proliferation and migration under nutrient-replete conditions and its loss preserves viability under glucose starvation. Whether this dual role can be exploited therapeutically remains to be determined and will require *in vivo* validation.

Discussion

In this study, we identified NCKAP1 as a regulator of glucose-starvation-induced, disulfide stress-driven cell death in an OSCC cell model. NCKAP1 and SLC7A11 were both higher in the two OSCC cell lines examined than in normal oral keratinocytes under their respective routine culture conditions. Culture under glucose-free conditions triggered rapid, non-apoptotic cell death that was attenuated by co-treatment with disulfide-reducing agents. Loss of NCKAP1 preserved cell viability and attenuated the depletion of intracellular free thiols, whereas NCKAP1 overexpression had the opposite effect. NCKAP1 manipulation did not materially alter total glutathione or GSSG, but produced modest changes in reduced GSH, the GSH/GSSG ratio and, after knockdown, the NADPH/$NADP^+$ ratio; therefore, the data argue against a major role of NCKAP1 in the upstream redox collapse but do not exclude a minor metabolic contribution. Beyond the stress setting, NCKAP1 knockdown also suppressed OSCC proliferation and migration under normal culture conditions. Together, these observations point to a dual role for NCKAP1 in this OSCC cell model.

Disulfidptosis was first defined as a death modality that occurs in SLC7A11-high cells deprived of glucose [16,17]. Under these conditions, NADPH becomes insufficient to reduce imported cystine, and the resulting disulfide stress disrupts the actin cytoskeleton [17]. Our OSCC model reproduced the central features of this process. Glucose starvation lowered the NADPH/$NADP^+$ ratio and, within hours, both depleted the total glutathione pool and shifted it toward the oxidized state, such that GSSG accumulated and the GSH/GSSG ratio fell by approximately 89% at 4 h. Free-thiol content fell in parallel. The cells became rounded and rapidly detached from the substrate. This death was not blocked by inhibitors of apoptosis, necroptosis, autophagy, or ferroptosis and was substantially, though not completely, prevented by co-treatment with DTT and TCEP. This pattern is consistent with disulfidptosis rather than with other established death pathways, although neither disulfide-crosslinking of cytoskeletal proteins nor morphological reorganization of the actin network was examined directly in our system. Removing cystine from the medium attenuated the phenotype, further supporting a requirement for cystine influx. We note that disulfide-bond formation was inferred from bulk free-thiol measurements and rescue by reducing agents rather than measured directly on individual proteins. Because NCKAP1 was originally identified as a disulfidptosis regulator in renal cancer, the contribution of NCKAP1 observed here is in part confirmatory. The contribution of the present work lies in extending this dependency to OSCC, showing that the effect of NCKAP1 is conditional on SLC7A11-mediated cystine import, and linking NCKAP1 to OSCC proliferation and migration under nutrient-replete conditions.

Silencing SLC7A11 abolished glucose-starvation-induced death. On this background, forced expression of NCKAP1 could not restore death. NCKAP1 therefore appears unable to drive this death process in the absence of SLC7A11-dependent cystine import. Manipulating NCKAP1 changed neither the size of the glutathione pool nor the amount of GSSG accumulated during starvation. Reduced GSH, the GSH/GSSG ratio and, in knockdown cells, the NADPH/$NADP^+$ ratio shifted slightly in the protective direction, but these shifts accounted for less than one tenth of the starvation-induced changes and were an order of magnitude smaller than the effects of the glucose-free condition itself. NCKAP1 is therefore not required for the metabolic collapse that precedes disulfide stress. The residual differences are more parsimoniously interpreted as a consequence rather than a cause, since cells with a less elaborate branched-actin network may present fewer oxidizable thiols and consume fewer reducing equivalents. Consistent with this interpretation, the free-thiol increment conferred by NCKAP1 knockdown under starvation was several-fold larger than the accompanying increment in reduced GSH, indicating that most of the preserved thiol pool was non-glutathione and presumably protein-associated. NCKAP1 is an established component of the WAVE regulatory complex, which couples Rac1 signaling

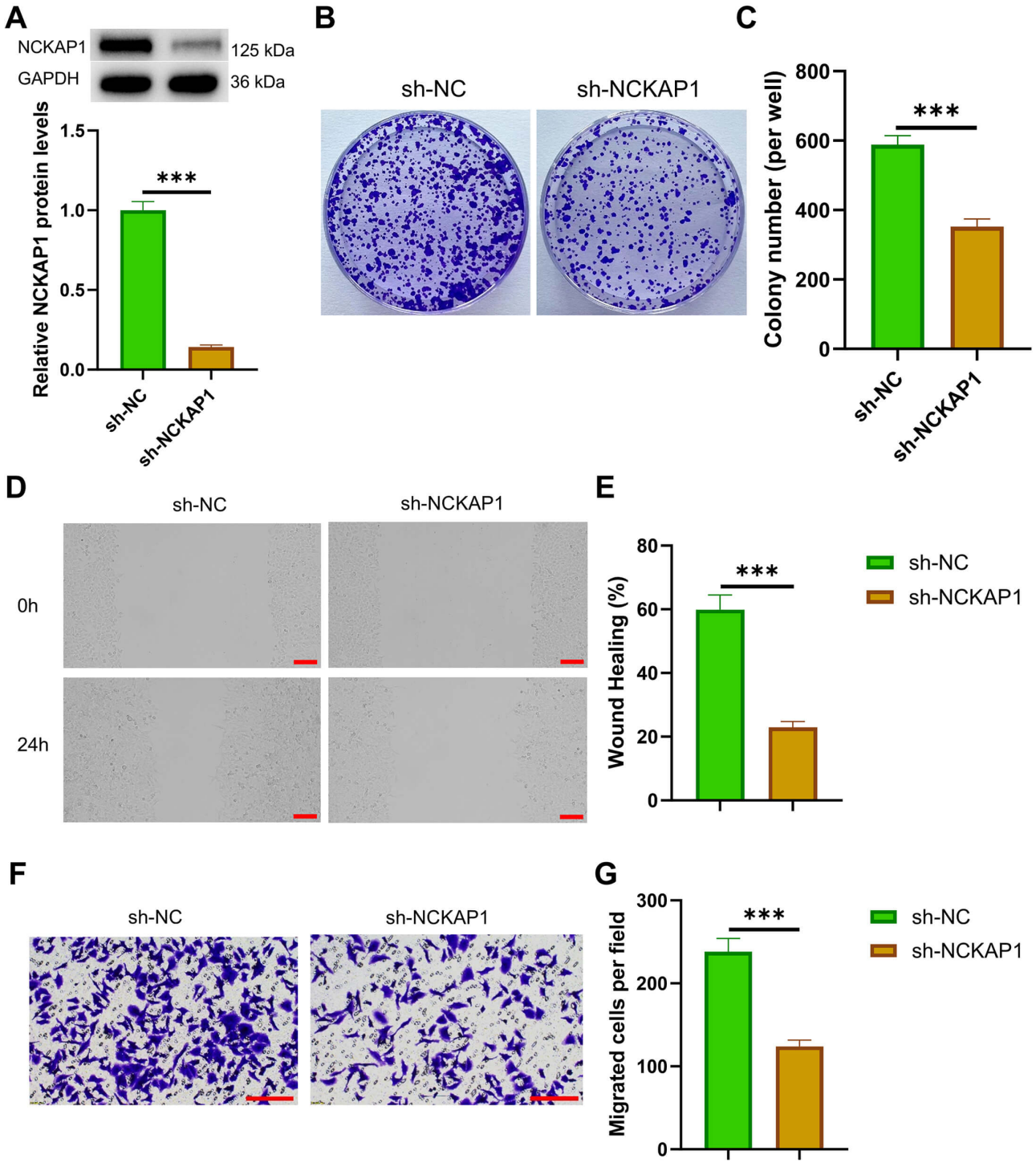

Fig. 7. NCKAP1 knockdown suppressed OSCC proliferation and migration under normal culture conditions. (A) Western-blot validation of NCKAP1 knockdown in the stable sh-NCKAP1 SCC-9 line. (B) Representative crystal-violet-stained colony-formation images (500 cells/well, 14 days, no scale bar, images show entire wells). (C) Quantification of colony number per well. (D) Representative wound-healing images at 0, 24 h (scale bar: 100 µm). (E) Quantification of wound-closure percentage. (F) Representative Transwell migration images (24 h, scale bar: 100 µm). (G) Quantification of migrated cells per field. Data are mean ± SD (n = 5). *** $p < 0.001$.

to Arp2/3- mediated branched actin polymerization [23,24]. We did not obtain imaging evidence of cytoskeletal reorganization in the present study, and the genetic data can only be interpreted in the light of the established molecular identity of NCKAP1. The finding that NCKAP1 knockdown preserved, and NCKAP1 overexpression further re-

duced, viability under glucose starvation is consistent with a role for WAVE-complex-associated cytoskeletal regulation in this process, consistent with the genome-wide screens in which loss of WAVE regulatory complex activity protected renal cancer cells from disulfide stress [16]. The cytoskeleton itself was not examined here, and this interpretation is therefore not established by our data. Taken together, these observations suggest that the contribution of NCKAP1 requires SLC7A11-dependent cystine stress, rather than occupying a defined position downstream of SLC7A11 in a linear pathway. NCKAP1 knockdown was also associated with a smaller net loss of free thiols under glucose starvation. One possible interpretation is that a more elaborate actin network provides additional substrate for thiol oxidation. Our data do not establish this directly, and we present it only as a hypothesis. The small parallel changes in reduced GSH and in the GSH/GSSG ratio are compatible with the same interpretation.

NCKAP1 knockdown reduced colony formation, wound closure, and transwell migration under nutrient-replete conditions. These findings are consistent with the known function of the WAVE complex in actin branching. The same protein thus appears to support malignant behavior during normal growth while also being required for the full loss of viability under metabolic stress. This combination is of interest because it raises the possibility that NCKAP1 influences these cells through more than one mechanism, a possibility that will need to be tested directly. We stress that this interpretation rests on *in vitro* observations and remains to be validated *in vivo*.

The glucose-replete control used here was the conventional complete medium in which the cells are routinely maintained, rather than a control prepared in the glucose-free basal medium with D-glucose added back. The two conditions therefore differed in basal formulation and in the use of dialyzed serum, in addition to D-glucose, and the phenotype should be attributed to the glucose-free culture condition as a whole rather than to the removal of glucose in isolation. This does not bear on the conclusions drawn about NCKAP1, because every comparison between si-NC and si-NCKAP1, between OE-NC and OE-NCKAP1, and across the SLC7A11-silenced backgrounds was made between cells cultured in the same medium for the same period, so that any difference in basal formulation or serum applies equally to both arms. It does, however, mean that the absolute magnitude of the death observed on transfer to glucose-free medium cannot be apportioned between glucose removal and the accompanying changes in medium composition. A glucose add-back-matched control, together with a compositional comparison of the two media, would be required to resolve this. Further, the effects of NCKAP1 and SLC7A11 manipulation on cell fate (Fig. 4E,F and Fig. 5B,D) were assessed with the CCK-8 assay, in which the WST-8 signal is generated by cellular dehydrogenase activity and therefore reports metabolic capacity rather than membrane integrity or cell death as such. Because the conditions studied here alter the cellular redox and metabolic state, a change in CCK-8 signal in these experiments cannot be attributed unambiguously to protection from death as distinct from preservation of metabolic activity. We have accordingly described these results as changes in cell viability or survival rather than as changes in cell death. Two considerations bear on their interpretation. First, the nature of the death process in this model was established separately, with LDH release and Annexin V/PI flow cytometry (Fig. 2B,D,E), readouts that report membrane integrity independently of metabolic activity. Second, within the genetic experiments the CCK-8 signal and the DTNB free-thiol content changed concordantly (Fig. 4E–H and Fig. 5B,C). These two readouts are not independent of the underlying redox state, however, and their concordance therefore does not formally separate protection from death from preservation of metabolic activity. Confirmation of the NCKAP1 effect with membrane-integrity or flow-cytometric readouts applied to the same genetic backgrounds would be required to make that distinction.

This study has several other limitations. The mechanistic experiments were performed exclusively in SCC-9 cells. CAL-27 was used only for the expression comparison in Fig. 1. The findings therefore describe a single OSCC cell model, and we do not generalise them to OSCC cells in general. Confirmation in additional OSCC lines will be required. Disulfide-bond formation was inferred from bulk free-thiol measurements and from rescue by reducing agents, rather than demonstrated directly on individual cytoskeletal proteins. In addition, alternative death modalities were probed with a single inhibitor at a single concentration and a single exposure time, and the pharmacological activity of each inhibitor was not verified with a positive control in our cells. A failure to rescue viability therefore indicates that these pathways are unlikely to be the dominant route of death under the conditions tested, but does not formally exclude their involvement. Specifically, disulfide-linked aggregation of cytoskeletal proteins such as ACTB, FLNA, MYH9 and TLN1 was not examined by non-reducing Western blotting, which would provide more definitive evidence for disulfidptosis. For this reason, we describe the death observed in the present study as disulfide stress-driven rather than as disulfidptosis throughout. Direct chemical-proteomic mapping of disulfide-crosslinked actin proteins was established in the original definition of disulfidptosis. In the present study, free-thiol depletion together with rescue by DTT and TCEP was used as a recognized surrogate readout supporting involvement of the same thiol-redox mechanism in OSCC. A further limitation is that we did not obtain morphological evidence of actin cytoskeleton reorganization. Imaging of filamentous actin at a magnification and cell density sufficient to delineate individual cell boundaries and quantify cytoskele-

tal parameters on a per-cell basis was not achievable with the instrumentation available for this study, and no F-actin imaging data are reported here. Any interpretation involving cytoskeletal regulation therefore rests on genetic manipulation of a core WAVE regulatory complex component together with the free-thiol and viability readouts, and not on direct visualization of the cytoskeleton. Such a contribution is described here as consistent with our data rather than as demonstrated. Confocal imaging with single-cell segmentation, together with non-reducing western blotting of cytoskeletal proteins, would be required to establish this step more directly. Also, the placement of NCKAP1 within the WAVE-Arp2/3 machinery is based on its established molecular role rather than on direct interaction data obtained here. Further, the expression comparison in Fig. 1 is subject to two limitations. The three lines were maintained in different routine media, namely DMEM/F12 with serum and hydrocortisone for SCC-9, high-glucose DMEM with serum for CAL-27, and a keratinocyte-specific medium with a proprietary growth supplement for HOK. Culture conditions are therefore a confounding factor that we did not control, and the differences observed describe the cells as routinely cultured rather than an intrinsic property of the malignant phenotype. A comparison performed in a common medium would be required before attributing the difference to tumour cell identity. In addition, the comparison was made at the cell-line level against a single normal keratinocyte line, which cannot represent the variability of normal oral epithelium. Tissue-level and survival analyses in OSCC patient cohorts remain to be performed. All functional readouts were obtained *in vitro*, and *in vivo* validation will be required to assess the therapeutic relevance of targeting NCKAP1 in OSCC. The positioning of NCKAP1 relative to SLC7A11 is based on the failure of NCKAP1 overexpression to restore death in SLC7A11-silenced cells, together with the quantitatively marginal effects of NCKAP1 on the starvation-induced metabolic changes. Because the shifts in reduced GSH and the GSH/GSSG ratio produced by NCKAP1 manipulation, although small, reached statistical significance, a minor contribution of NCKAP1 to redox homeostasis cannot be formally excluded, and we do not claim that NCKAP1 is entirely without metabolic consequence. A negative rescue result does not by itself establish a linear pathway order, and we did not obtain evidence that SLC7A11 regulates NCKAP1 expression or interacts with it directly. The relationship we describe should therefore be regarded as a functional dependency rather than a demonstrated upstream-downstream relationship. We therefore describe the contribution of NCKAP1 as requiring SLC7A11-dependent cystine stress and as consistent with a role for WAVE-complex-associated cytoskeletal regulation, and we avoid asserting it a downstream position within a linear pathway. A further limitation concerns the use of DTT and TCEP. Both agents reduce extracellular cystine to cysteine, which can enter cells independently of SLC7A11 and does not require NADPH-dependent reduction. Because the reducing agents were added at the onset of glucose starvation, their protective effects may reflect prevention of disulfide stress at the extracellular level rather than reversal of established intracellular stress. Delayed addition of reducing agents after the stress has developed, together with direct quantification of cystine and cysteine in the medium and in cell lysates, will be required to distinguish these possibilities.

Conclusion

In summary, our results identify NCKAP1 as a contributor to glucose-starvation-induced, disulfide stress-driven cell death in an OSCC cell model and to their proliferation and migration. These findings add the WAVE regulatory complex component NCKAP1 to the factors linked to this death modality and identify it as a candidate for further study in OSCC.

Availability of Data and Materials

The data that support the findings of this study are available from the corresponding author upon reasonable request.

Author Contributions

WWH, JSY and SM designed the research study. WLL, JRH and YPS performed the research. WWH, WLL and SM analyzed the data. WWH has been involved in drafting the manuscript and all authors contributed to important editorial changes in the manuscript. All authors read and approved the final manuscript. All authors have participated sufficiently in the work and agreed to be accountable for all aspects of the work.

Ethics Approval and Consent to Participate

Not applicable.

Acknowledgment

Not applicable.

Funding

This research was supported by 2025 Program of Research Projects in Traditional Chinese Medicine Sciences (Grant No.2025385).

Conflict of Interest

The authors declare no conflict of interest.

References

[1] Pekarek L, Garrido-Gil MJ, Sánchez-Cendra A, Cassinello J, Pekarek T, Fraile-Martinez O, et al. Emerging histological and serological biomarkers in oral squamous cell carcinoma: Applications in diagnosis, prognosis evaluation and personalized therapeutics (Review). Oncology Reports. 2023; 50: 213. https://doi.org/10.3892/or.2023.8650

[2] Muralidharan S, Nikalje M, Subramaniam T, Koshy JA, Koshy AV, Bangera D. A Narrative Review on Oral Squamous Cell Carcinoma. Journal of Pharmacy & Bioallied Sciences. 2025; 17: S204–S206. https://doi.org/10.4103/jpbs.jpbs_593_25

[3] Dong L, Xue L, Cheng W, Tang J, Ran J, Li Y. Comprehensive survival analysis of oral squamous cell carcinoma patients undergoing initial radical surgery. BMC Oral Health. 2024; 24: 919. https://doi.org/10.1186/s12903-024-04690-z

[4] Stawarz K, Bieńkowska-Pluta K, Galazka A, Gorzelnik A, Durzynska M, Misiak-Galazka M, et al. Clinicopathologic Predictors of Survival Following Oral Cancer Surgery: A Retrospective Cohort Study. Cancers. 2025; 17: 2454. https://doi.org/10.3390/cancers17152454

[5] Bjerkli IH, Jetlund O, Karevold G, Karlsdóttir Á, Jaatun E, Uhlin-Hansen L, et al. Characteristics and prognosis of primary treatment-naïve oral cavity squamous cell carcinoma in Norway, a descriptive retrospective study. PloS One. 2020; 15: e0227738. https://doi.org/10.1371/journal.pone.0227738

[6] Listl S, Jansen L, Stenzinger A, Freier K, Emrich K, Holleczek B, et al. Survival of patients with oral cavity cancer in Germany. PloS One. 2013; 8: e53415. https://doi.org/10.1371/journal.pone.0053415

[7] Azzi L, Celesti F, Chiaravalli AM, Shaik AKB, Shallak M, Gatta A, et al. Novel vaccination strategies based on optimal stimulation of $CD4^+$ T helper cells for the treatment of oral squamous cell carcinoma. Frontiers in Immunology. 2024; 15: 1387835. https://doi.org/10.3389/fimmu.2024.1387835

[8] Bai R, Meng Y, Cui J. Therapeutic strategies targeting metabolic characteristics of cancer cells. Critical Reviews in Oncology/hematology. 2023; 187: 104037. https://doi.org/10.1016/j.critrevonc.2023.104037

[9] Bai J, Wu L, Wang X, Wang Y, Shang Z, Jiang E, et al. Roles of Mitochondria in Oral Squamous Cell Carcinoma Therapy: Friend or Foe? Cancers. 2022; 14: 5723. https://doi.org/10.3390/cancers14235723

[10] Liang L, Luo C, Dong S, Jia Z, Zhao L, Tang J, et al. Lipid homeostasis dysregulation in oral cancer drives metabolic reprogramming and offers novel diagnostic and therapeutic opportunities. Discover Oncology. 2025; 16: 1613. https://doi.org/10.1007/s12672-025-03299-0

[11] Peng F, Liao M, Qin R, Zhu S, Peng C, Fu L, et al. Regulated cell death (RCD) in cancer: key pathways and targeted therapies. Signal Transduction and Targeted Therapy. 2022; 7: 286. https://doi.org/10.1038/s41392-022-01110-y

[12] Saxena R, Welsh CM, He YW. Targeting regulated cell death pathways in cancers for effective treatment: a comprehensive review. Frontiers in Cell and Developmental Biology. 2024; 12: 1462339. https://doi.org/10.3389/fcell.2024.1462339

[13] Hadian K, Stockwell BR. The therapeutic potential of targeting regulated non-apoptotic cell death. Nature Reviews. Drug Discovery. 2023; 22: 723–742. https://doi.org/10.1038/s41573-023-00749-8

[14] Lee E, Song CH, Bae SJ, Ha KT, Karki R. Regulated cell death pathways and their roles in homeostasis, infection, inflammation, and tumorigenesis. Experimental & Molecular Medicine. 2023; 55: 1632–1643. https://doi.org/10.1038/s12276-023-01069-y

[15] Jin X, Jin W, Tong L, Zhao J, Zhang L, Lin N. Therapeutic strategies of targeting non-apoptotic regulated cell death (RCD) with small-molecule compounds in cancer. Acta Pharmaceutica Sinica. B. 2024; 14: 2815–2853. https://doi.org/10.1016/j.apsb.2024.04.020

[16] Liu X, Nie L, Zhang Y, Yan Y, Wang C, Colic M, et al. Actin cytoskeleton vulnerability to disulfide stress mediates disulfidptosis. Nature Cell Biology. 2023; 25: 404–414. https://doi.org/10.1038/s41556-023-01091-2

[17] Liu X, Zhuang L, Gan B. Disulfidptosis: disulfide stress-induced cell death. Trends in Cell Biology. 2024; 34: 327–337. https://doi.org/10.1016/j.tcb.2023.07.009

[18] Jiang Y, Sun M. SLC7A11: the Achilles heel of tumor? Frontiers in Immunology. 2024; 15: 1438807. https://doi.org/10.3389/fimmu.2024.1438807

[19] Jyotsana N, Ta KT, DelGiorno KE. The Role of Cystine/Glutamate Antiporter SLC7A11/xCT in the Pathophysiology of Cancer. Frontiers in Oncology. 2022; 12: 858462. https://doi.org/10.3389/fonc.2022.858462

[20] TeSlaa T, Ralser M, Fan J, Rabinowitz JD. The pentose phosphate pathway in health and disease. Nature Metabolism. 2023; 5: 1275–1289. https://doi.org/10.1038/s42255-023-00863-2

[21] Li T, Song Y, Wei L, Song X, Duan R. Disulfidptosis: a novel cell death modality induced by actin cytoskeleton collapse and a promising target for cancer therapeutics. Cell Communication and Signaling : CCS. 2024; 22: 491. https://doi.org/10.1186/s12964-024-01871-9

[22] Bieling P, Rottner K. From WRC to Arp2/3: Collective molecular mechanisms of branched actin network assembly. Current Opinion in Cell Biology. 2023; 80: 102156. https://doi.org/10.1016/j.ceb.2023.102156

[23] Ding B, Yang S, Schaks M, Liu Y, Brown AJ, Rottner K, et al. Structures reveal a key mechanism of WAVE regulatory complex activation by Rac1 GTPase. Nature Communications. 2022; 13: 5444. https://doi.org/10.1038/s41467-022-33174-3

[24] Han KA, Ko J. Orchestration of synaptic functions by WAVE regulatory complex-mediated actin reorganization. Experimental & Molecular Medicine. 2023; 55: 1065–1075. https://doi.org/10.1038/s12276-023-01004-1

[25] Xiao Y, Mendez PL, Hiepen C, Jatzlau J, Knaus P. NCKAP1 coordinates focal adhesion and adherens junction dynamics in endothelial barrier maintenance and angiogenesis. iscience. 2026; 29: 115716. https://doi.org/10.1016/j.isci.2026.115716

[26] Zhu A, Zong Y, Wei S, Li Y, Fan Y, Liu S, et al. Pan-cancer Analysis of the Disulfidptosis-related Gene NCKAP1 and Its Prognostic Value for Lung Adenocarcinoma. Journal of Cancer. 2023; 14: 3351–3367. https://doi.org/10.7150/jca.88650